Research Square

Preprints are preliminary reports that have not undergone peer review.
They should not be considered conclusive, used to inform clinical practice,
or referenced by the media as validated information.

Development and Characterization of Antimicrobial Persian Gum-Based Films Incorporated with Date Waste-Derived Carbon Quantum Dots and Shirazi Thyme Essential Oil

Aref Adeli mosabbeb
Shahid Beheshti University of Medical Sciences
Negin Majdi
Islamic Azad University
Samira Dakhili
Shahid Beheshti University of Medical Sciences
Mehdi Farhoodi
Shahid Beheshti University of Medical Sciences
Hedayat Hosseini
Shahid Beheshti University of Medical Sciences
Farzaneh Rouhani
Shahid Beheshti University
Saeedeh Shojaee-Aliabadi
s_shojaee@sbmu.ac.ir

Shahid Beheshti University of Medical Sciences

Article

Keywords: Persian gum, Carbon dots, Date waste, Shirazi thyme essential oil, Antimicrobial film

Posted Date: November 16th, 2026

DOI: https://doi.org/10.21203/rs.3.rs-11307878/v1

License: This work is licensed under a Creative Commons Attribution 4.0 International License.
Read Full License

Additional Declarations: No competing interests reported.

Development and Characterization of Antimicrobial Persian Gum-Based Films Incorporated with Date Waste-Derived Carbon Quantum Dots and Shirazi Thyme Essential Oil

Aref Adeli mosabbeb[1], Negin Majdi[2], Samira Dakhili[1], Mehdi Farhoodi[1], Hedayat Hosseini[1], Farzaneh Rouhani[*3], Saeedeh Shojaee-Aliabadi[*1]

[1]Department of Food Science and Technology, National Nutrition and Food Technology Research Institute, Faculty of Nutrition Sciences and Food Technology, Shahid Beheshti University of Medical Sciences, Tehran, Iran

[2]Faculty of Medical Sciences, Science and Research Branch, Islamic Azad University, Tehran, Iran

[3]Department of Inorganic Chemistry, Shahid Beheshti University, Tehran, Iran

E mail addresses:

Aref Adeli Mosabbeb: arefadeli7@gmail.com

Negin Majdi: neginmajdi9999@gmail.com

Samira Dakhili: Samiradakhili@gmail.com

Mehdi Farhoodi: mehdi.farhoodi@gmail.com

Hedayat Hosseini: hedayat@sbmu.ac.ir

Corresponding authors:

* s_shojaee@sbmu.ac.ir

Food Science and Technology Department

Faculty of Nutrition and food Science

Shahid Beheshti University

P.O. Box 19395-4741, Tehran, Iran

Tel/Fax: +98 21 22376

* f_rouhani@sbu.ac.ir

Department of Inorganic Chemistry

Faculty of Chemistry

Shahid Beheshti University
Tel/Fax: +98 21 22376

Development and Characterization of Antimicrobial Persian Gum-Based Films Incorporated with Date Waste-Derived Carbon Quantum Dots and Shirazi Thyme Essential Oil

Abstract

This study developed multifunctional Persian gum (PG)-based active films incorporating carbon quantum dots (CQDs) synthesized from date seed waste and *Zataria multiflora* essential oil (ZMEO). CQD incorporation markedly influenced the physicochemical and mechanical performance of the films. Among the investigated concentrations, 1% CQDs provided the most favorable mechanical properties, resulting in the highest tensile strength, elongation at break, and elastic modulus, whereas increasing the CQD concentration to 1.5% reduced these parameters. Increasing CQD content also enhanced UV-shielding capacity, with the 1.5% CQD film showing nearly complete attenuation of radiation below 350 nm. The film containing both CQDs and ZMEO exhibited the highest DPPH radical-scavenging activity (63.48%) and showed antimicrobial activity against Staphylococcus aureus, Escherichia coli, Listeria monocytogenes, and Salmonella typhimurium. Increasing the CQD concentration reduced ZMEO release at 4, 25, and 37 °C, indicating that CQDs influenced the migration behavior of the essential oil within the PG matrix. Kinetic analysis indicated predominantly Fickian diffusion based on the Korsmeyer–Peppas model, while the Peleg model provided the best overall description of the release data (R^2 > 0.9). These findings demonstrate the potential of waste-derived CQDs as multifunctional components in biodegradable active films, although further validation in real food systems is required before practical packaging applications can be established.

Keywords: Persian gum, Carbon dots, Date waste, Shirazi thyme essential oil, Antimicrobial film.

1. Introduction

In recent years, ensuring food safety and food quality through the supply chain has become one of the most important challenges for the food industry, which has greatly highlighted the need to develop innovative packaging solutions. Active packaging is one such technology that has gained a special place due to its effectiveness in preventing food spoilage and increasing shelf life by inhibiting the growth of microorganisms and preventing destructive biochemical reactions (1). In this regard, antimicrobial films have received much attention due to their ability to prevent microbial contamination and reduce food waste, and the use of functional nanomaterials, include quantum dots, as effective additives to enhance the performance of active films is increasing. However, the packaging industry's reliance on synthetic plastics continues to cause serious environmental problems as most of these materials are disposable and not naturally degradable (2, 3). Consequently, biodegradable packaging materials based on plant and animal biopolymers have attracted widespread attention as a desirable alternative to synthetic plastics because they are environmentally friendly, renewable and sustainable resources (4).

Persian gum (PG) is a natural and inexpensive biopolymer that is extracted from the Scots almond tree (*Amygdalus scoparia*), a species native to Iranian regions, and has been considered as a suitable option for the production of biobased and biodegradable films due to its abundance, availability, and desirable properties. This gum mainly consists of polysaccharides, a significant proportion of which are galactopyranosyl and arabinofuranosyl units that play a fundamental role in its hydrocolloid behavior (5). PG has a water-soluble part with good solubility and an insoluble part that dissolves slightly in hot water. In addition, PG is used in the food industry as a stabilizer, emulsifier, and film-forming agent due to its high water-absorption capacity and appropriate

rheological properties. However, like many natural gums, the resulting films may face challenges such as low mechanical strength, moisture sensitivity, and limited stability, which highlights the need to improve its structure for advanced packaging applications (6).

Zataria multiflora boiss, also known as "Shirazi thyme", is a plant of the *Laminaceae* family that grows only in Iran, Pakistan, and Afghanistan. Among the 215 known species of this plant in the world, only 14 species are distributed in the flora of Iran. This plant is used to preserve and flavor many products due to its strong antimicrobial properties and pleasant taste in the food industry. Phenolic compounds present in this plant, such as carvacrol and thymol, are mainly responsible for the antimicrobial activity of this plant against a wide range of bacteria and fungi (7). In order to increase the use of essential oils and plant extracts for food preservation, strategies are required to control the antibacterial effect, mask the strong aroma and flavor, and enhance stability against degradation by environmental conditions during processing and storage (8). In this regard, active antimicrobial packaging and coatings are proposed as a promising solution. This type of packaging can increase the safety and quality of products by reducing the risk of contamination (9).

Carbon quantum dots (CQDs), as carbon nanomaterials with a size of less than 10 nm, have attracted much attention due to their properties such as water solubility, suitable biocompatibility, low toxicity, and broad functional capabilities such as antioxidant, antibacterial, and photostability properties (1). The graphitic core structure and the presence of various functional groups such as oxygen and nitrogen on the surface of these carbon dots provide them with unique photoluminescence properties and UV-shielding ability, making them a suitable candidate for the development of novel applications, especially in active packaging films (10). The optical and behavioral qualities of CQDs depend on the synthesis route, temperature, time, and type of carbon precursor, which allows for the tuning of their properties. In the synthesis methods, both “top-

down" and "bottom-up" routes are used, but green and sustainable syntheses such as hydrothermal, microwave, and ultrasonic synthesis, which lead to the formation of CQDs from natural precursors, are of more interest due to their environmental compatibility. These methods follow the steps of dehydration, polymerization, carbonization, and passivation, and allow the production of stable and efficient carbon dots without the need for hazardous chemicals (11).

In addition, the use of agricultural waste as a sustainable carbon source for the production of CQDs has increased, and date seeds are one of the most valuable of these sources. Date seeds (DS) are rich in fiber, minerals, and phenolic compounds with antioxidant, anticancer, and cardiovascular protective activities (12). These bioactive compounds can regulate the chemical structure and functional groups of the resulting CQDs during the carbonization process, leading to the production of highly efficient and biocompatible carbon dots (13). Converting date waste into functional nanomaterials adds value, and CQDs produced from this natural source are in line with the principles of sustainable development. They also show significant potential for use in active food packaging to extend product shelf life and enhance food safety, as well as for the development of biocompatible materials. These advantages have led to the emergence of date waste–derived carbon dots as an innovative, low-cost, and environmentally friendly option for both research and industrial applications (14).

While Persian gum (PG) has been investigated as a natural film-forming polysaccharide and essential oils have been widely studied as bioactive agents in biopolymer films, the functional role of biomass-derived carbon quantum dots (CQDs) within multicomponent active-film systems remains an area requiring further investigation. Agricultural residues such as wheat bran (15), orange peel (16), onion peel (17), coffee ground (18), lemon peel (19), rice residue (20) and coconut husks (21) and coconut husks (21) have been used as carbon precursors for CQD synthesis.

Date seeds have also been reported as a precursor for CQD production; therefore, the novelty of the present study does not rely solely on the use of date seed waste as a carbon source. Rather, the distinctive aspect of this work lies in investigating date seed-derived CQDs within a Persian gum/Zataria multiflora essential oil (ZMEO) film system and evaluating their contribution to both film functionality and essential-oil release behavior.

Active packaging films based on biodegradable polymers have received considerable attention as sustainable alternatives to conventional plastic materials. However, the development of multifunctional films that simultaneously provide adequate mechanical performance, bioactive functionality, and controlled release of active compounds remains challenging. In particular, the incorporation of nanofillers may alter not only the structural and barrier properties of the polymer matrix but also the mobility and release behavior of incorporated essential oils. Therefore, understanding these combined effects is important for designing active films with balanced physicochemical and functional performance.

Based on these considerations, the present study was designed to investigate the multifunctional role of date seed-derived CQDs in a Persian gum/ZMEO film system. Particular attention was given to determining whether variations in CQD concentration could influence the physicochemical, mechanical, optical, antioxidant, and antimicrobial characteristics of the films, while also affecting the migration behavior of ZMEO from the polymer matrix. Evaluating these responses within the same film system provides a more integrated assessment of the contribution of CQDs than approaches focusing on a single functional property.

Accordingly, the novelty of the present study lies in evaluating date seed-derived CQDs not merely as reinforcing or bioactive additives, but as multifunctional components capable of simultaneously influencing the physicochemical, mechanical, optical, antioxidant, antimicrobial, and release

characteristics of a Persian gum/ZMEO active-film system. Therefore, this study aimed to develop Persian gum-based active films incorporating date seed-derived CQDs and ZMEO and to systematically evaluate the effects of CQD concentration on the physicochemical, barrier, mechanical, optical, antioxidant, and antimicrobial properties of the resulting films. In addition, the release behavior of ZMEO was investigated at different temperatures and analyzed using multiple kinetic models to elucidate the dominant release characteristics. This integrated approach was intended to provide a comprehensive assessment of the multifunctional role of date seed-derived CQDs in biodegradable active-film systems.

2. Materials and methods

2.1. Materials

PG was obtained from a reputable herbalist in Kurdistan Province. Tween 80, 2,2- diphenyl-1-picrylhydrazyl (DPPH), calcium chloride, sodium chloride, ethanol and glycerol were provided by Merck Co. (Darmstadt, Germany). Date seed powder (DS) was purchased from a Pourhamzeh manufacturing CO. (Shiraz, Iran) and ZMEO was supplied by Barij CO. (Kashan, Iran). Plate Count Agar (PCA) and Trypticase Soy Broth (TSB) were bought from Merck Co (Darmstadt, Germany).

2.2. Bacterial strains

Staphylococcus aureus ATCC 25923; *Escherichia coli* ATCC 25922; *Salmonella typhimurium* ATCC 14028 and *Listeria monocytogenes* ATCC 7644 were provided by Iranian Research Organization for Science and Technology (Tehran, Iran). Stock cultures of the studied bacteria were grown in TSB at 37 ℃ for 24 h before the tests.

2.3. Methods

Selected experimental procedures for film preparation, physicochemical characterization, and essential-oil release analysis were adapted, where applicable, from the study conducted by Dakhili et al. (23). These procedures were modified as necessary to accommodate the Persian gum-based film system incorporating date seed-derived carbon quantum dots (CQDs) and Zataria multiflora essential oil (ZMEO). The experimental conditions and analytical methods employed in the present study are described in detail in the following subsections.

2.3.1. Preparation of CDs

CDs were prepared using a one-step hydrothermal method using a DS solution (22). As shown schematically in Fig 1, for the preparation of CQDs, 2 g of DS was dissolved in 100 mL of deionized water with stirring and placed in a polytetrafluoroethylene (Teflon) lined stainless steel reactor (150 mL) followed by the reactor was heated to 200 ℃ for 6 h in an oven. After cooling, the reaction product was centrifuged at 10,000 rpm for 20 min to remove the unreacted material. The supernatant was filtered through a Whatman membrane filter (25 mm diameter nylon filter, pore size: 0.22 μm, Mn, Germany). After that, the filtrate was stored in a refrigerator before further testing. The morphology and particle-size distribution of the prepared CQDs were characterized by transmission electron microscopy (TEM). Their incorporation into the PG-based film system was further evaluated through spectroscopic, optical, colloidal-stability, and morphological analyses of the resulting film-forming systems and films, as described in the following sections.

2.3.2. Film preparation

Persian gum-based films were prepared using previously reported film-forming procedures (1, 6), with modifications to the essential-oil incorporation and film-casting steps based on the method described by Dakhili et al. (23).

186 The PG granule with white color was powdered using a laboratory mill device and was sieved in
187 a shaker device (Retsch, USA) via a sieve with a mesh number of 100. 2 g of PG powder was
188 added to 100 mL of sterilized distilled water and stirred with glycerol (50% of the gum) for 5h at
189 40 ˚C on a heater stirrer with a magnet. In order to reduce the brittleness of the films, glycerol was
190 added as a plasticizer during the preparation of the composite film. The suspension was centrifuged
191 (Eppendorf 5810, Germany) for 20 min at 3500 g. After removing the insoluble phase, the purified
192 PG solution was prepared. After that, four different concentrations of CDs (0, 0.5, 1 and 1.5 wt%)
193 were gradually added to the solution and stirred vigorously for 2 h. These four films were named
194 as Control (0%), CD1 (0.5%), CD2 (1%), and CD3 (1.5%). The optimal concentration was selected
195 based on the functional activity (such as UV protection, antioxidant, and antibacterial properties)
196 of the resulting nanoparticles through experiments. After that, the final film solutions were
197 achieved by adding 1.5 % (v/v) essential oil and Tween 80 (0.1 % v/v in quantities proportional to
198 the essential oil) to the optimal concentration of PG-CDs and finally homogenized by ultrasound
199 (Topsonics, Iran) at 250 W, 20 Hz for 4 min. Then, 75 ml of each dispersion was poured into Teflon
200 plates with a surface area of 153.94 cm^2 and subsequently placed into the incubator for 24 h at 35
201 ℃ to dry. The dried film was removed from the plate and placed at 25 °C and 50% relative
202 humidity for at least two days before further experiments (1, 6, 23).

203 **2.3.3. Thickness**

204 Film thickness was measured via a manual micrometer (Mitutoyo, Japan) averaging ten different
205 positions of each film sheet to the nearest 0.001 mm.

206 **2.3.4. Water solubility (WS)**

Briefly, four pre-weighed samples of each treatment (2 × 2 cm^2) were immersed in 50 ml of distilled water under constant agitation for 6 h at 25 ℃ and then filtered. The papers containing undissolved particles were dried at 110 ℃ to constant weight and the water solubility was calculated using Eq (1).

$$WS\ (\%) = \frac{(\text{Initial dry weight}) - (\text{Dry weight of undissolved material})}{\text{Initial dry weight}} \times 100 \quad (1)$$

2.3.5. Fourier-transform infrared spectroscopy (FTIR)

ATR-FTIR analysis of nanocomposites was carried out through a Perkin-Elmer FTIR spectrophotometer (Spectrum 1, USA) within a range of 500–4000 cm^{-1} using a resolution of 4 cm^{-1} to observe the structural interactions within the samples.

2.3.6. Mechanical properties

According to a previous study (24) mechanical parameters including Tensile strength (TS), elongation at break (EB) and elastic modulus (EM) of preconditioned films (1.5 cm × 10 cm) were measured at 25 ˚C with a Testometric Machine M350- 10CT (Testometric Co., Ltd., Rochdale, Lancs., England). Film samples wit an initial grip length of 50 mm and cross-head speed of 50 mm/min were used for testing. Mentioned values were calculated according to Eq (2), Eq. (3), and Eq. (4):

$$TS = \frac{\text{Maximum force}}{(\text{Film width}) \times (\text{Film thickness})} \quad (2)$$

$$EB\ (\%) = \frac{(\text{Maximum length before breaking}) - (\text{Initial length})}{\text{Initial length}} \quad (3)$$

$$EM = \frac{TS}{EB\%} \times 100 \quad (4)$$

2.3.7. Water vapor permeability (WVP)

227 WVP of samples was determined at ambient temperature and RH = 75 % gradient. The test cups
228 (with a surface area of 0.00287 m^2) containing 100 g anhydrous calcium chloride (0 % RH) were
229 sealed by test films and placed in saturated sodium chloride desiccators (75 % RH). The difference
230 in RH value of the inner and outer atmosphere of cups corresponds to a driving pressure of 1753.55
231 Pa (25). The cups were weighed at 1 h intervals over a 10 h period and the weight gain was
232 recorded. Water vapor transmission rate (WVTR) and WVP were calculated based on Eq. (5) and
233 Eq. (6):

234 $$\text{WVTR} = \frac{\text{The weight gain versus time slope } \left(\frac{g}{s}\right)}{\text{Exposed surface area of film } (m^2)} \quad (5)$$

235 $$\text{WVP} = \text{WVTR} \times \frac{\text{Film thickness (m)}}{\text{Difference of pressure between the inner and outer sides of the cup (Pa)}} \quad (6)$$

236 **2.3.8. Zeta potential**

237 The surface charge (zeta potential) of 2% PG, 0.5% CD + 2% PG, 1% CD + 2% PG, and 1.5% CD
238 + 2% PG solutions was characterized using a nanoparticle analyzer (Zetasizer Nano ZSP, Malvern
239 Instrument Ltd., Worcestershire, UK) (26).

240 **2.3.9. Color**

241 Film samples were subjected to a colorimeter (Minolta CR 300 Series, Minolta Camera Co., Ltd.,
242 Osaka, Japan) for color evaluation, and the color parameters were expressed as L* (lightness: black
243 to white), a* (greenness to redness), and b* (blueness to yellowness). The total color difference
244 (ΔE*) was calculated according to Eq. (7):

245 $$\Delta E^* = \sqrt{((\Delta L^*)^2 + (\Delta a^*)^2 + (\Delta b^*)^2)} \quad (7)$$

where ΔL*, Δa*, and Δb* are the differences between the color parameter of the samples and those of the white standard (L* = 93.92, a* = - 1.3 and b* = 0.23).

2.3.10. Transparency and light transmission

The absorption spectrum was determined by a UV–Vis spectrophotometer (UV-5200 PC, Shanghai Yuantong Instrument Co., LTD), with scanning range of 190-900 nm. Fluorescence spectrometer (Perkin Elmer model Lambda 2, Germany) was used to measure emission spectra at different excitation wavelengths to analyze the changes of fluorescence intensity of samples. The UV barrier and transparency properties of the film were evaluated by determining the light transmittance and absorbance at 280 nm (T_{280}) and 660 nm (T_{660}) (22, 27).

2.3.11. TEM (Transmission electron microscopy)

The morphological features of the sample were characterized by TEM. The dilute aqueous solution of the sample was sonicated for 15 min by sonicator. Then, one drop of the sample was dropped onto Formvar carbon film on a copper grid 300 mesh (EMS-USA) and dried thoroughly at room temperature. The sample was observed by transmission electron microscopy (Carl Zeiss-Germany) at an accelerating voltage of 100 kV, and Image J was used to calculate the particle size distribution (28, 29).

2.3.12. SEM (Scanning electron microscopy)

The surface morphology of the film samples was observed by SEM. The film samples (2cm × 2cm) were sputter coated with Au/Pd under high vacuum and morphology was observed by scanning electron microscope (SEM) (Hitachi, S-3400N) at an accelerating voltage of 15 kV (30).

2.3.13. Antioxidant properties

The antioxidant activities of films were evaluated with a standard antioxidant assay using DPPH according to Hanani et al. (2018) with some modifications (31). Film samples (2 × 2 cm2) were added to 20 ml ethanol and kept for 20 min at 25 ˚C. Subsequently, 0.1 ml film extract was added to 3.9 ml of 0.01 mmol/L DPPH solution, mixed evenly and placed in the dark. After 30 min, the absorbance of the mixture was measured at 517 nm. The percentage of DPPH free radical scavenging activity was calculated according to Eq. (8):

$$\text{DPPH radical scavenging activity (\%)} = \left(\frac{\text{Abs DPPH} - \text{Abs Sample}}{\text{AbsDPPH}}\right) \times 100 \quad (8)$$

2.3.14. Antimicrobial properties

The antimicrobial activities of films incorporated with ZMEO against selected bacteria were evaluated through the disc diffusion method (32). Film samples were aseptically cut into 6 mm diameter discs and placed on plates containing MHA. The medium had been previously seeded with 100 μL of an overnight broth culture containing approximately 10^7 CFU/ml of the test bacteria. The diameter of the growth inhibition zones was measured after 24 h of incubation at 37˚C in triplicate for each formulation.

2.3.15. Release test

The experimental procedure for investigating essential-oil release and the approach used for kinetic modeling were adapted from Dakhili et al. (23), with modifications to account for the composition of the PG–CQD–ZMEO films and the experimental conditions employed in the present study.

The The film samples with dimensions (2 × 2 cm^2) were immersed in 20 ml of distilled water. The release kinetics of the essential oil from these structures were measured for 48 h at 4, 25 and 37

°C. All release experiments were performed in triplicate for each formulation at each temperature, and the results are expressed as mean ± standard deviation. At different intervals, the absorbance of each sample at 265 nm, as the wavelength with the highest absorption for ZMEO, was measured by a UV–Vis spectrophotometer (Perkin Elmer model Lambda 2, Germany). Furthermore, to describe the release behavior and the dominant mechanism involved in the release of the essential oil from the matrix of films to food simulant, various mathematical equations (Eq. (9), Eq. (10), Eq. (11), Eq. (12), and Eq. (13)) were used:

- Zero order model: $M_\infty - M_t = kt$ (9)
- First order model: $\text{Log}(M_t/M_\infty) = kt$ (10)
- Higuchi model: $M_t/M_\infty = kt^{1/2}$ (11)
- Korsmeyer-Peppas model: $\text{Log}(M_t/M_\infty) = \log k + n \text{ Log } t$ (12)

where M_t and M_∞ are the absolute cumulative amount of released ZMEO at time t and infinite time; k is the characteristics of the macromolecular network system; and n is the release exponent indicative of the mechanism of release. For the thin film, if $n < 0.5$, the release mechanism is usually based on Fick diffusion, and $0.5 < n < 1.0$ shows an anomalous transport diffusion, and $n = 1$ indicates an erosion-controlled release (33).

- Peleg model is demonstrated by Eq. (13):

$$M_t = t/k_1 + k_2 t \quad (13)$$

where M_t is the cumulative amount of released ZMEO at time t, k_1 is the Peleg rate constant that is inversely related to the mass transfer rate at the beginning of the process, and k_2 is a constant of the model that is related to the asymptotic value, which can be related to the equilibrium value ($1/M_\infty$ where M_∞ is the amount of ZMEO released at equilibrium)

2.3.16. Statistical analysis

Data analysis was carried out by SPSS (version 26) software. One-way analysis of variance (ANOVA) and subsequent Duncan's multiple range tests were applied to determine any significant differences among the treatments at a 95% confidence level.

3. Results and discussion

Our pre-test studies showed that films containing at least 0.5% CD exhibit reasonable properties and excellent uniformity. Concentrations of 0.5, 1, and 1.5 % were also considered to investigate the properties of this class of films.

3.1. Characterization of CQDs

The morphology and particle-size distribution of the date seed-derived CQDs were evaluated by TEM (Fig. 2). As shown in Fig. 2A, the CQDs exhibited a predominantly spherical morphology and were relatively well dispersed, with no obvious extensive aggregation. Particle-size analysis further showed an average diameter of approximately 3.07 nm (Fig. 2B), confirming the successful formation of nanoscale carbon dots under the applied hydrothermal synthesis conditions. The relatively small particle size and dispersion observed by TEM support their suitability for incorporation into the PG-based film-forming system.

3.2. Thickness

Table 1 shows the physical properties of PG/CQDs and its films containing different CQD concentrations (0.5–1.5 wt%) and ZMEO with or without CQD (E and CQD/E). The various barrier and mechanical properties are evaluated by the thickness of the films. The thickness of the PG film decreased after the addition of CQDs, indicating that the CQDs were tightly dispersed within the PG film (29). The average thickness of the PG film without CQDs was 62.12 ± 3.46 μm

and increased significantly to 68.52 ± 2.7 μm at 1.5 % of ZMEO concentration, because the EOs were added as a dispersed phase (oil droplets) to the aqueous/polymer matrix, which increased the solid content in the film and consequently the thickness (34).

3.3. WS

The water solubility analysis for the synthesized films was studied and displayed in Table 1. Due to the hydrophilic nature and high aqueous dispersibility of CQDs synthesized from DS powder, increasing their concentration enhanced the water solubility of PG-based films. However, the incorporation of ZMEO partially counteracted this effect by increasing the hydrophobicity of the film matrix. Kalanidhi and Nagaraaj (2022) previously reported that the solubility of chitosan/PVP films was significantly increased by the presence of NCDs and orange peel extract, and this result was due to the presence of more polar functional groups in the film solution containing these compounds (35).

3.4. WVP

WVP is a vital factor in determining the shelf life of food products. The ability of biopolymer films to act as a barrier against water vapor transmission is an important factor that determines the quality and shelf life of food. So that, on the one hand, high barrier packaging is preferred when water vapor exchange is not desirable (for example, dry products), but on the other hand, medium to high water vapor transmission is considered desirable in some products to prevent water condensation inside the packaging (for example, fruits and vegetables) (32). For this reason, the WVP of different films was measured (Table 1). The results of this test showed that the addition of CQDs synthesized from DS powder to PG-based films caused a significant ($p<0.05$) increase in the amount of WVP compared to the control film (1 and 1.5%). This behavior can be attributed to the

hydrophilic nature of these nanoparticles and the presence of polar functional groups such as hydroxyl and carboxyl on their surface, which increase water vapor absorption and swelling of the polymer film network. The increase in swelling led to an increase in the distance between PG chains and facilitated the passage of water molecules through the film matrix (22).

In contrast, the addition of ZMEO to PG films caused a significant decrease in WVP, which was attributed to the hydrophobic nature of the main essential oil compounds such as thymol and carvacrol. The presence of these compounds was associated with reducing the tendency of the film to absorb water vapor and limiting the passage of water vapor through the film structure (7). In films containing both CQDs and ZMEO, the WVP value showed an intermediate behavior; So that the WVP of these films was lower than the samples containing CQDs and higher than the films containing only essential oil. This behavior indicates a competitive effect between the hydrophilic nature of CQDs and the hydrophobic nature of the essential oil. In addition, the presence of CQDs probably helped to improve the dispersion of essential oil in the PG matrix and prevented the creation of micropores, which led to the stability of the film structure and the control of water vapor permeability.

In line with our findings, Min et al. (2022) reported increased WVP of gelatin composite film by the addition of potato skin CD (2 and 4 wt%) (2). The CD-added films decreased water vapor barrier (i.e., increased WVP) may be due to the surface hydrophilic functional groups of the CD (36). However, Murugan and Nilsuwan (2024) reported that adding Guava leaf powder carbon dots to active fish gelatin/chitosan blend film can effectively prevent the entry and penetration of water molecules. The inclusion of carbon dots in the chitosan film matrix reliably provides a difficult path for water molecules in the film network. As a result, both the hydrophilicity of the film and the WVP of the final films decreased (37).

3.5. Mechanical properties

The strength and mechanical integrity of food packaging films play a crucial role in maintaining product safety and preventing breakage or leakage during storage and distribution processes (38). The mechanical properties (Young's modulus (EM), tensile strength (TS), and elongation at break (EB)) of PG film and its nanocomposites incorporated with CQDs and ZMEO are shown in Table 1. The results showed that by increasing the concentration of CQDs to 1%, the TS, EB, and EM of the packaging films increased significantly ($p<0.05$). So that the TS and EB values increased from 0.357 ± 0.021 and 17.826 ± 4.814 in the control samples to 1.361 ± 0.232 and 34.717 ± 2.364 in the 1% CQDs samples, respectively. This improvement in mechanical properties can be attributed to the proper dispersion of nanoparticles in the polymer matrix and the creation of effective interactions between the functional groups on the surface of CQDs and polymer chains, which leads to better stress transfer and strength of the film structure. The uniform distribution of nanoparticles at this concentration, in addition to increasing the strength and modulus, also improved the flexibility of the film (39).

By increasing the concentration of CQs to 1.5%, a simultaneous decrease in all three mechanical parameters was observed (TS= 1.005 ± 0.154, EB= 28.496 ± 5.182, EM= 21.479 ± 3.77), which is probably due to the aggregation of nanoparticles and their non-uniform distribution in the polymer matrix (40). This aggregation creates stress concentration areas and reduces the effective interaction between the nanofiller phase and the polymer, resulting in a weakening of the mechanical properties. Therefore, the results show that a concentration of 1% CQDs as the optimal value provides the greatest improvement in the mechanical performance of the films.

Furthermore, the addition of ZMEO to the polymer films increased all three parameters, which is attributed to the interaction of the active compounds of the essential oil with the polymer chains

and improved structural integrity of the matrix (41). However, the highest and most favorable mechanical properties were obtained for the films containing the combination of CQDs and ZMEO, indicating the existence of a synergistic effect between these two additives. In this system, CQDs as a reinforcing agent improve stress transfer, and ZMEO enhances the interaction between phases by reduce the aggregation of nanoparticles and increase their uniform dispersion; as a result, a more integrated structure with higher mechanical performance is obtained, making it suitable for food packaging applications (42).

In an investigation done by Mei et al. (2022) had been observed that the TS of the film added with CDs decreased, but the EB increased significantly. Probably due to the hydrophilicity of CDs, the increase in water content of the film led to a decrease in TS. In addition, CDs may combine with sericin and glycerol to form hydrogen bonds, reduce protein-protein interactions and increase the mobility of the polymer segment, thus increase the elongation at break (40).

3.6. FTIR

FTIR spectra are usually used to determine the major functional groups of carbohydrates (31). This test was performed on control films containing different concentrations of CQDs from DS (Fig 3). In the FTIR spectrum of films, the presence of COOH or the bonding vibration of CH_3 represent the carboxylate groups of uronic acid residues which trigger signal at around 1422 cm^{-1}. Signals at 1602-1620 cm^{-1} were also attributed to anhydride components produced via carboxyl groups, or the presence of bound water or carboxyl groups (43). Also, asymmetric and symmetric stretching patterns between C-H bonds and asymmetric CH_2 functional groups give rise to other detectable signals (2925 cm^{-1}). The formation of ether bonds (C-O-C) as well as stretching and bending vibrations of C=O and N-H bonds in the esterified structure was evidenced by a significant

422 increase in the FTIR spectra in the range of 1050-1200 cm^{-1} and a new absorption peak at 1220
423 cm^{-1} (6).

424 Strong and broad signals in the range of 3240-3320 cm^{-1} were observed in all layers, which were
425 probably due to the stretching vibration of hydroxyl, and the signal related to the stretching
426 vibration of C-OH and C-O-C ether functional groups (986 cm^{-1}) appeared in the FTIR spectrum.
427 In addition, a new peak at 3460 cm^{-1}, which represents the bending vibration of hydroxyl in the
428 complexed film, was formed (44). The increase in the concentration of CQDs from 0.5% to 1.5%
429 results in a reduction in the intensity of the –OH band and an increase in its width. This indicates
430 the formation of stronger hydrogen bonds between the hydroxyl groups of PG and the surface
431 functional groups of the CQDs (–OH and –COOH). Also, a slight shift in the range of 1600–1700
432 cm^{-1} is observed with increasing percentage of CDs, which can be due to the presence of carbonyl
433 and carboxyl groups on the surface of CQDs and their interaction with the polymer matrix (1, 45).
434 Overall, the absence of new peaks in the nanocomposite film spectrum suggests that no new
435 covalent bonds are formed, indicating that the structural modification process is primarily physical,
436 and the original chemical structure of the polymer is preserved.

437 **3.7. Zeta potential**

438 The zeta potential of food packaging film solutions is performed to evaluate surface charge, system
439 stability, component compatibility, and predict final film quality (46). The zeta potential of PG-
440 based packaging film solutions, including the control sample and samples containing 0.5, 1, and
441 1.5 % CQDs extracted from DS, was measured to evaluate the surface charge and colloidal stability
442 of the system. All samples were found to have negative zeta potentials, which can be attributed to
443 the presence of anionic PG functional groups and surface oxygenated CQD groups. The control
444 sample (without CQDs) showed an average zeta potential value of about -30.0 mV, which indicates

moderate stability of the suspension and the presence of electrostatic repulsion between polymer chains. Adding 0.5% CQDs decreased the zeta potential value to approximately -30.2 mV, that indicate a slight increase in negative surface charge and improved system stability.

The increase in the concentration of CQDs to 1% resulted in a zeta potential of -51.8 mV, indicating a significant increase in electrostatic repulsion and high stability of the suspension. This behavior could be due to a more uniform distribution of carbon quantum dots and their stronger interaction with the Persian gum matrix. In the sample containing 1.5% carbon quantum dots, the zeta potential value decreased to -75.5 mV, which shows the highest negative charge among the samples and shows the very high stability of the colloidal system.

The direct relationship between the absolute value of zeta potential and the concentration of CQDs indicates the effective role of nanoparticles in increasing the negative surface charge and preventing particle aggregation. This can lead to a more uniform distribution of the nanofiller phase in the film-forming solution and ultimately improving the microstructure and physical-mechanical properties of the final films. Based on the colloidal stability criteria and the study by Zemljič et al. (2020), the zeta potential value in stable systems is greater than -30 mV, as a result, samples containing 1 and 1.5% CQDs have very favorable stability (47).

3.8. Optical properties

The surface color and light transmittance of the PG-based films are shown in Table 2. This test was performed to compare between different films with different concentrations of CQDs. The pure PG film was transparent, flexible and colorless to the naked eye, while the nanocomposite films containing ZMEO showed a slightly yellow to light brown appearance. The addition of CQDs decreased the brightness (L value) of the PG film, changing from 77.51 ± 0.01 to 52.19 ±

467 0.98 ($p < 0.05$). While it increased the redness (a value) and yellowness (b value) of the PG, which
468 was attributed to the brown color of the CQDs. As a result, the overall film color difference (ΔE)
469 increased significantly with the addition of CQDs. Similar to our results, Riahi et al. (2022)
470 observed that the use of chitosan-based carbon quantum dots in CMC-based films could reduce
471 the brightness of the film and increase its redness, yellowness and ΔE (46).

472 According to Table 2, to evaluate the UV-blocking properties and film transparency, the film light
473 transmission was measured at wavelengths of 280 nm (T_{280}) and 660 nm (T_{660}). The results showed
474 that the addition of CQDs to PG-based packaging films significantly reduced the light transmission
475 in the range of 190–900 nm, such that this reduction was completely dependent on the CQDs
476 concentration (Fig 4). The control film exhibited the highest light transmission across the entire
477 spectral range. Conversely, an increase in CQDs concentration from 0.5% to 1.5% resulted in a
478 sharp decrease in light transmission within the UV region (200-400 nm). UV blocking generally
479 helps preserve food quality, especially that of high-fat foods susceptible to photocatalytic oxidation
480 and UV light can accelerate the loss of organoleptic properties (odor, color, and taste) and
481 nutritional quality of food (48). The film containing 1.5% CQDs showed almost negligible
482 transmission at wavelengths below 350 nm, indicating the high ability of these particles to absorb
483 and block UV radiation. This behavior is mainly attributed to $\pi \rightarrow \pi^*$ and $n \rightarrow \pi^*$ electronic
484 transitions in the carbon structure and the presence of functional groups on the surface of the CQDs
485 (37). In addition, in the visible region (400–700 nm), a gradual decrease in light transmission was
486 observed with increasing CQDs concentration, which is attributed to the increase in turbidity and
487 light scattering in the polymer matrix. At higher wavelengths (700-900 nm), no significant
488 difference was observed between the samples and all films had similar light transmittance values,
489 indicating selective absorption of CQDs in the short-wave UV and visible regions. Overall PG

films reinforced with CQDs, especially at concentrations of 1 and 1.5%, have effective light shielding properties and can be considered a suitable option for packaging light-sensitive food products.

3.9. SEM

The structure of the composite film is influenced by the compatibility between the nanoparticles and the polymer matrix and the way these particles are distributed in the polymer matrix. The surface and cross-sectional SEM images of the PG-based films are shown in Fig. 5. All the films showed a dense surface without cracks or aggregation due to the homogeneous dispersion of CQDs in the polymer matrix. The SEM results showed that the CQD was uniformly dispersed in the film, indicating good compatibility between CQDs and PG, which is mainly due to the hydrophilicity of CQDs (46).

3.10. Antioxidant activity

The films' antioxidant activity was assessed through a DPPH scavenging assay (Table. 3). The results of the DPPH assay showed that increasing the concentration of CQDs had a significant effect on increasing antioxidant activity, such that by increasing the concentration from 0.5 to 1.5%, the percentage of free radical scavenging increased significantly ($p<0.05$). This behavior can be attributed to the increase in the number of surface-active functional groups in CQDs that are capable of donating electrons or hydrogen and neutralizing DPPH free radicals. Also, the more uniform distribution and better interaction of quantum dots with the film matrix at higher concentrations can facilitate the access of radicals to the active antioxidant sites (49).

On the other hand, the addition of ZMEO could significantly increase the antioxidant activity of the packaging films, with essential oils having greater effects than CQDs. In addition, the synergy between CQDs and antioxidant compounds of essential oils in CD/E films lead to enhanced free

radical scavenging performance. As reported by Dashipour et al. (2015) and Sharififar et al. (2007), the antioxidant activity of ZMEO is attributed to phenolic compounds such as thymol, carvacrol, and γ-terpinene, which are involved in quenching free radicals (50, 51). However, according to the results of Moradi et al. (2016), despite the increase in the concentration of ZMEO in zein films from 2% to 3% w/v, the DPPH radical scavenging activity did not show a significant change, and the slight increase observed (from about 27% to 31%) was attributed to the minimal interactions in the protein matrix (52).

3.11. Antimicrobial properties

In this study, the antimicrobial effects of the film samples (Control, CD1, CD2, CD3, E and CD/E) against *Staphylococcus aureus*, *Escherichia coli*, *Salmonella typhimurium* and *Listeria monocytogenes* were evaluated using the agar disk diffusion method and the results are shown in Table 3. As expected, the film containing PG (Control) showed no antimicrobial activity against any of the tested microorganisms. The films containing CQDs had different activities against Gram-positive and Gram-negative bacteria (Table 3). The results showed that the CD1 film had no significant effect on *E. coli* or *L. monocytogenes*. However, increasing the concentration of CQDs enhanced the antimicrobial effect, reaching a maximum at 1.5% CQDs. Among the selected bacteria, *E. coli* showed the highest resistance, while *S. aureus* was the most sensitive bacterium to the nanocomposite films. As reported by other researchers, the antimicrobial properties of CQDs are mainly attributed to their ability to generate reactive oxygen species (ROS) from their surface, which exert significant bacteriostatic effects on a wide range of microorganisms (4). Increased cell membrane permeability, induction of oxidative stress, and damage to the genetic structures of microorganisms are among the proposed mechanisms for the antimicrobial action of ROS. Also,

this can inactivate cellular proteins, induce lipid peroxidation, disrupt mitochondrial function, and gradually destroy cell membranes, ultimately leading to microbial cell death (53).

The antimicrobial activity of CQDs is influenced by several factors, including the type of bacteria, the concentration of quantum dots, their morphology, surface charge, and the nature of the functional groups present on their surface. As expected, the antimicrobial activity of synthesized CQDs against Gram-positive bacteria is generally higher than against Gram-negative bacteria due to differences in cell wall structure (54). In line with this study, Ezzati et al. (2022) demonstrated that films containing CQDs derived from glucose exhibited stronger antibacterial activity against Gram-positive bacteria than Gram-negative bacteria. Consequently, Gram-positive bacteria are more susceptible to the harmful effects of ROS due to the lack of an outer membrane (55). In contrast, Ghadiri Alamdari et al. (2023) showed that the highest effect of synthesized CQDs was observed on gram-negative (*P. aeruginosa*) and the least effect on gram-positive (*L. monocytogenes*) (45).

The addition of ZMEO to PG-based films was also found to significantly increase their antimicrobial activity compared to the control film. This can be due to the presence of the essential oil's bioactive compounds, such as carvacrol and thymol, which are dominant in ZMEO and can disrupt the phospholipid bilayer of the cell membrane and damage enzyme systems (56). In previous studies such as Dashipour et al. (2015), it was confirmed that the antibacterial effects of CMC films containing ZMEO against five pathogenic Gram-positive and Gram-negative bacteria were more effective on gram-positive bacteria than on gram-negative bacteria due to the impermeability of the outer membrane of gram-negative bacteria to lipophilic components (50). Furthermore, the highest inhibition of microbial growth was observed in films containing a combination of CQDs and ZMEO, suggesting a synergistic interaction between these two

antimicrobial agents. This synergy could be due to the facilitation of the penetration of essential oil compounds into microbial cells in the presence of CQDs and also the intensification of oxidative damage to vital cellular structures, which overall leads to an increase in the antimicrobial efficacy of the films. However, further research is needed to investigate the antimicrobial activity of CQDs on mold species.

3.12. Release test

The release of ZMEO in PG-films with different concentrations of CQD in water was evaluated at three temperatures of 4, 25 and 37 ˚C. Fig. 6. shows the cumulative release curve of ZMEO/PG-films and illustrates the effects of time, temperature and CQD concentration on the release pattern of ZMEO. The general trend of the diffusion rate of essential oil into water was similar at all temperatures. Initially, an increase in the migration rate, after which the amount of these changes is minimized and finally reaches equilibrium. The notable point in these graphs is that the time required to reach equilibrium and the percentage of release through the rapid phase were different at different CQD concentrations. According to these results, increasing the temperature from 4 to 25 ℃, resulted in an increase in the release trend, which then decreased at 37 ˚C. On the other hand, with increasing CQD concentration at all three temperatures studied, the release rate decreased significantly.

Controlled release from the film at a specific rate over a period of time is important for increasing the product's shelf life. Therefore, modelling the experimental data and determining the mass transfer parameters may be necessary for potential product applications (57). For this reason, the experimental data obtained from the ZMEO release study were fitted with different models (Table 2). In order to study the main mechanism of ZMEO release from the nanocomposite film structure, the n-index of the Korsmeier-Peppas model was investigated for the time period of the sorting

process. Since the n-index for all samples at temperatures of 4, 25, and 37 °C was less than 0.5, it can be concluded that the main release mechanism was Fick diffusion. Dakhili et al. (2024) observed that the mechanism of Release of *Satureja Khuzestanica* Jamzad essential oil from fish gelatin/succinic anhydride starch nanocomposite films was Ficki diffusion (23). The data obtained from ZMEO release were also fitted with the Peleg model (Table 4). Unlike the Peleg and Korsmeyer-Peppas models that could predict the amount at equilibrium with time tending to infinity, the other models studied were valid only for the first stage of ZMEO release. The results showed that a wide range of values from the experimental data could be estimated by the Peleg model with the highest values of correlation coefficient (R^2) greater than 0.9. Therefore, this model was selected as the best model to describe the kinetics of ZMEO release at different temperatures. The parameters of the Peleg model are shown in Table 2. In general, the k_1 and k_2 values of the studied films increased with increasing CQD concentration from 4 to 37 °C, indicating the controlling effect of CQDs on the release rate.

The decrease in essential oil release rate as the concentration of CQDs in the films increases can be attributed to a set of structural and intermolecular mechanisms. The presence of CQDs as a nanofiller increases the tortuosity of the diffusion path and reduces the free volume in the polymer matrix. This results in a decrease in the effective diffusion coefficient of volatile essential oil compounds (58). In addition, the presence of active functional groups such as hydroxyl and carboxyl on the surface of CQDs leads to the formation of hydrogen bonds with the polysaccharide chains of PG and also the phenolic compounds of the essential oil, which limits the mobility of the polymer chains and the ability of essential oil molecules to migrate. Also, the absorption and retention of some of the essential oil compounds on the surface of CQDs can result in a gradual and slower release of the essential oil (48). In general, denser film microstructure, the

reinforcement of the polymer network, and the increased barrier effect resulting from the increased concentration of CQDs play a key role in reducing the release of the essential oil.

The release rate increased with temperature due to greater polymer chain mobility and, consequently, greater ZMEO migration from the matrix to the simulator at 25 °C. However, the decrease in release rate between 25 and 37 °C is probably due to a dominant change in release control mechanisms. In this temperature range, the strengthening of intermolecular interactions between the phenolic compounds of the essential oil and the functional groups on the surface of carbon quantum dots, along with the structural rearrangement of the polymer matrix and the reduction of the effective swelling of the film, can lead to increased retention of the essential oil in the film structure. In addition, increasing temperature may reduce the effective solubility of some essential oil compounds in the polymer phase or increase surface evaporation, thereby reducing the effective concentration gradient for intramatrix diffusion (59). Also, the addition of CQD was found to control the release of SKEO from nanocomposite films at all temperatures. The film containing 1.5 wt% CQD exhibited the lowest ZMEO release. Peleg model parameters also confirm this phenomenon: the highest k_1 was observed in the 1.5% CQD film at 4 °C, and the lowest value was observed in the 0.5% CQD film at 37 °C. Ranjbarian, Pourfathi, and Almasi (2019) reported similar results for the enhanced release of cinnamon essential oil from active sodium caseinate nanocomposite films at 37 °C compared to 25 and 4 °C (60). Another study also showed that the use of a 3D printer could play an important role in improving the retention of cinnamon essential oil in a two-layer film containing corn starch/gelatin (61).

4. Conclusion

PG films containing date seed-derived CQDs and ZMEO were developed and characterized. Among the CQD concentrations tested, 1% CQDs produced the highest tensile strength, elongation

at break, and elastic modulus, whereas increasing the concentration to 1.5% reduced these mechanical parameters. CQD incorporation also improved UV blocking and antioxidant activity, while increasing water vapor permeability; ZMEO reduced the latter effect. The film containing both CQDs and ZMEO showed the highest DPPH radical-scavenging activity (63.48%) and the largest inhibition zones among the tested formulations for the four evaluated bacteria. These results demonstrate that the combined formulation provided multiple functional properties within the tested film system.

Release experiments showed that increasing CQD concentration reduced ZMEO release at 4, 25, and 37 °C. The Korsmeyer–Peppas analysis indicated Fickian diffusion ($n < 0.5$), while the Peleg model provided the best fit among the evaluated models ($R^2 > 0.9$). Thus, the main contribution of this study is the integration of date seed-derived CQDs into a PG/ZMEO film and the characterization of their effects on mechanical, optical, antioxidant, antimicrobial, and release properties. Because the present work was conducted under laboratory conditions, further studies in real food systems, including migration, safety, storage stability, and application performance, are required before practical food-packaging use can be established.

CRediT authorship contribution statement

Aref Adeli mosabbeb: Conceptualization, Methodology, Software, Investigation, Resources, Writing original draft, Visualization, Project administration.
Negin Majdi: Methodology, Software, Investigation.
Samira Dakhili: Methodology, Software, Investigation.
Mehdi Farhoodi: Project administration, Investigation, Data curation.
Hedayat Hosseini: Methodology, Validation, Writing review & editing, Supervision, Data curation.
Farzaneh Rouhani: Project administration, Investigation, Software.

Saeedeh Shojaee-Aliabadi: Conceptualization, Methodology, Software, Formal analysis, Validation, Investigation, Resources, Data curation, Writing review & editing, Supervision, Project administration, Funding acquisition

Declaration of competing interest

The authors declare that they have no known competing financial interests or personal relationships that could have appeared to influence the work reported in this paper.

Acknowledgement

The authors would like to thank the Shahid Beheshti University of Medical Science, Tehran, Iran for the support of this research project.

Data Availability

The datasets generated and/or analyzed during the current study are available from the corresponding author on reasonable request

References

1. Sul Y, Ezati P, Rhim J-W. Preparation of chitosan/gelatin-based functional films integrated with carbon dots from banana peel for active packaging application. International Journal of Biological Macromolecules. 2023;246:125600.

2. Min S, Ezati P, Rhim J-W. Gelatin-based packaging material incorporated with potato skins carbon dots as functional filler. Industrial Crops and Products. 2022;181:114820.

3. Ezati P, Roy S, Rhim J-W. Pectin/gelatin-based bioactive composite films reinforced with sulfur functionalized carbon dots. Colloids and Surfaces A: Physicochemical and Engineering Aspects. 2022;636:128123.

4. Kousheh SA, Moradi M, Tajik H, Molaei R. Preparation of antimicrobial/ultraviolet protective bacterial nanocellulose film with carbon dots synthesized from lactic acid bacteria. International Journal of Biological Macromolecules. 2020;155:216-25.

5. Najafian N, Aarabi A, Nezamzadeh-Ejhieh A. Evaluation of physicomechanical properties of gluten-based film incorporated with Persian gum and Guar gum. International Journal of Biological Macromolecules. 2022;223:1257-67.

6. Pak ES, Ghaghelestani SN, Najafi MA. Preparation and characterization of a new edible film based on Persian gum with glycerol plasticizer. Journal of food science and technology. 2020;57(9):3284-94.

7. Ghasemi S, Javadi NHS, Moradi M, Khosravi-Darani K. Application of zein antimicrobial edible film incorporating Zataria multiflora boiss essential oil for preservation of Iranian ultrafiltered Feta cheese. African Journal of Biotechnology. 2015;14(24):2014-21.

8. Nazari M, Majdi H, Milani M, Abbaspour-Ravasjani S, Hamishehkar H, Lim L-T. Cinnamon nanophytosomes embedded electrospun nanofiber: Its effects on microbial quality and shelf-life of shrimp as a novel packaging. Food Packaging and Shelf Life. 2019;21:100349.

9. Fadiji T, Rashvand M, Daramola MO, Iwarere SA. A review on antimicrobial packaging for extending the shelf life of food. Processes. 2023;11(2):590.

10. Barman BK, Nagao T, Nanda KK. Dual roles of a transparent polymer film containing dispersed N-doped carbon dots: A high-efficiency blue light converter and UV screen. Applied surface science. 2020;510:145405.

11. Moradi M, Molaei R, Kousheh SA, T. Guimarães J, McClements DJ. Carbon dots synthesized from microorganisms and food by-products: active and smart food packaging applications. Critical Reviews in Food Science and Nutrition. 2023;63(14):1943-59.

12. Alananbeh KM, Bouqellah NA, Al Kaff NS. Cultivation of oyster mushroom Pleurotus ostreatus on date-palm leaves mixed with other agro-wastes in Saudi Arabia. Saudi journal of biological sciences. 2014;21(6):616-25.

13. Yao Y-Y, Gedda G, Girma WM, Yen C-L, Ling Y-C, Chang J-Y. Magnetofluorescent carbon dots derived from crab shell for targeted dual-modality bioimaging and drug delivery. ACS applied materials & interfaces. 2017;9(16):13887-99.

14. Farshbaf M, Davaran S, Rahimi F, Annabi N, Salehi R, Akbarzadeh A. Carbon quantum dots: recent progresses on synthesis, surface modification and applications. Artificial cells, nanomedicine, and biotechnology. 2018;46(7):1331-48.

15. John TS, Yadav PK, Kumar D, Singh SK, Hasan SH. Highly fluorescent carbon dots from wheat bran as a novel drug delivery system for bacterial inhibition. Luminescence. 2020;35(6):913-23.

16. Prasannan A, Imae T. One-pot synthesis of fluorescent carbon dots from orange waste peels. Industrial & Engineering Chemistry Research. 2013;52(44):15673-8.

17. Bandi R, Gangapuram BR, Dadigala R, Eslavath R, Singh SS, Guttena V. Facile and green synthesis of fluorescent carbon dots from onion waste and their potential applications as sensor and multicolour imaging agents. RSC advances. 2016;6(34):28633-9.

18. Wang L, Li W, Wu B, Li Z, Wang S, Liu Y, et al. Facile synthesis of fluorescent graphene quantum dots from coffee grounds for bioimaging and sensing. Chemical Engineering Journal. 2016;300:75-82.

19. Tyagi A, Tripathi KM, Singh N, Choudhary S, Gupta RK. Green synthesis of carbon quantum dots from lemon peel waste: applications in sensing and photocatalysis. RSC advances. 2016;6(76):72423-32.

20. Qi H, Teng M, Liu M, Liu S, Li J, Yu H, et al. Biomass-derived nitrogen-doped carbon quantum dots: highly selective fluorescent probe for detecting Fe3+ ions and tetracyclines. Journal of colloid and interface science. 2019;539:332-41.

21. Chunduri L, Kurdekar A, Patnaik S, Dev BV, Rattan TM, Kamisetti V. Carbon quantum dots from coconut husk: evaluation for antioxidant and cytotoxic activity. Materials Focus. 2016;5(1):55-61.

22. Ezati P, Rhim J-W, Molaei R, Rezaei Z. Carbon quantum dots-based antifungal coating film for active packaging application of avocado. Food Packaging and Shelf Life. 2022;33:100878.

23. Dakhili S, Yekta R, Zade SV, Mohammadi A, Hosseini SM, Shojaee-Aliabadi S. Release kinetic modeling of Satureja Khuzestanica Jamzad essential oil from fish gelatin/succinic anhydride starch nanocomposite films: The effects of temperature and nanocellulose concentration. Food Chemistry. 2024;439:138152.

24. Zhang D, Chen L, Cai J, Dong Q, Din Z-u, Hu Z-Z, et al. Starch/tea polyphenols nanofibrous films for food packaging application: From facile construction to enhance mechanical, antioxidant and hydrophobic properties. Food Chemistry. 2021;360:129922.

25. Beristain-Bauza S, Mani-López E, Palou E, López-Malo A. Antimicrobial activity and physical properties of protein films added with cell-free supernatant of Lactobacillus rhamnosus. Food control. 2016;62:44-51.

26. Yu K, Zhou L, Huang H, Xu J, Li Y, Yu W, et al. The improvement of water barrier property in gelatin/carboxymethyl cellulose composite film by electrostatic interaction regulation and its application in strawberry preservation. Food Chemistry. 2024;450:139352.

27. Wen F, Li P, Zhang Y, Zhong H, Yan H, Su W. Preparation, characterization of green tea carbon quantum dots/curcumin antioxidant and antibacterial nanocomposites. Journal of Molecular Structure. 2023;1273:134247.

28. Fan K, Zhang M, Fan D, Jiang F. Effect of carbon dots with chitosan coating on microorganisms and storage quality of modified-atmosphere-packaged fresh-cut cucumber. Journal of the Science of Food and Agriculture. 2019;99(13):6032-41.

29. Bao J, Hu Y, Farag MA, Huan W, Wu J, Yang D, et al. Carbon dots, cellulose nanofiber, and essential oil nanoemulsion from Torreya grandis aril added to fish scale gelatin film for tomato preservation. International Journal of Biological Macromolecules. 2023;245:125482.

30. Wen F, Li P, Yan H, Su W. Turmeric carbon quantum dots enhanced chitosan nanocomposite films based on photodynamic inactivation technology for antibacterial food packaging. Carbohydrate Polymers. 2023;311:120784.

31. Hanani ZN, Yee FC, Nor-Khaizura M. Effect of pomegranate (Punica granatum L.) peel powder on the antioxidant and antimicrobial properties of fish gelatin films as active packaging. Food Hydrocolloids. 2019;89:253-9.

32. Shojaee-Aliabadi S, Hosseini H, Mohammadifar MA, Mohammadi A, Ghasemlou M, Ojagh SM, et al. Characterization of antioxidant-antimicrobial κ-carrageenan films containing Satureja hortensis essential oil. International journal of biological macromolecules. 2013;52:116-24.

33. Dammak I, de Carvalho RA, Trindade CSF, Lourenço RV, do Amaral Sobral PJ. Properties of active gelatin films incorporated with rutin-loaded nanoemulsions. International journal of biological macromolecules. 2017;98:39-49.

765 34. Kong I, Degraeve P, Pui LP. Polysaccharide-based edible films incorporated with essential
766 oil nanoemulsions: Physico-chemical, mechanical properties and its application in food
767 preservation—A review. Foods. 2022;11(4):555.
768 35. Kalanidhi K, Nagaraaj P. N-doped carbon dots incorporated chitosan/polyvinylpyrrolidone
769 based polymer film for advanced packaging applications. Chemical Physics Letters.
770 2022;805:139960.
771 36. Yadav S, Mehrotra G, Bhartiya P, Singh A, Dutta P. Preparation, physicochemical and
772 biological evaluation of quercetin based chitosan-gelatin film for food packaging. Carbohydrate
773 polymers. 2020;227:115348.
774 37. Murugan G, Nilsuwan K, Prodpran T, Ponnusamy A, Rhim J-W, Kim JT, et al. Active Fish
775 Gelatin/Chitosan Blend Film Incorporated with Guava Leaf Powder Carbon Dots: Properties,
776 Release and Antioxidant Activity. Gels. 2024;10(4):281.
777 38. Ezati P, Rhim J-W. Fabrication of quercetin-loaded biopolymer films as functional
778 packaging materials. ACS Applied Polymer Materials. 2021;3(4):2131-7.
779 39. Sadegh-Hassani F, Nafchi AM. Preparation and characterization of bionanocomposite
780 films based on potato starch/halloysite nanoclay. International journal of biological
781 macromolecules. 2014;67:458-62.
782 40. Mei S, Fu B, Su X, Chen H, Lin H, Zheng Z, et al. Developing silk sericin-based and carbon
783 dots reinforced bio-nanocomposite films and potential application to litchi fruit. Lwt.
784 2022;164:113630.
785 41. Sattariazar S, Arsalani N, Ebrahimi SN. Biological assessment of synthesized carbon dots
786 from polyphenol enriched extract of pomegranate peel, incorporated with Mentha piperita essential
787 oil. Materials Chemistry and Physics. 2023;294:126981.

42. Hosseini M, Razavi S, Mousavi M. Antimicrobial, physical and mechanical properties of chitosan-based films incorporated with thyme, clove and cinnamon essential oils. Journal of food processing and preservation. 2009;33(6):727-43.

43. Tabatabaei SD, Ghiasi F, Gahruie HH, Hosseini SMH. Effect of emulsified oil droplets and glycerol content on the physicochemical properties of Persian gum-based edible films. Polymer Testing. 2022;106:107427.

44. Abbasi S. Challenges towards characterization and applications of a novel hydrocolloid: Persian gum. Current Opinion in Colloid & Interface Science. 2017;28:37-45.

45. Alamdari NG, Almasi H, Moradi M, Akhgari M. Characterization of carbon quantum dots synthesized from vinasse and date seeds as agro-industrial wastes. Waste and Biomass Valorization. 2023;14(11):3689-703.

46. Riahi Z, Rhim J-W, Bagheri R, Pircheraghi G, Lotfali E. Carboxymethyl cellulose-based functional film integrated with chitosan-based carbon quantum dots for active food packaging applications. Progress in Organic Coatings. 2022;166:106794.

47. Zemljič LF, Plohl O, Vesel A, Luxbacher T, Potrč S. Physicochemical characterization of packaging foils coated by chitosan and polyphenols colloidal formulations. International Journal of Molecular Sciences. 2020;21(2):495.

48. Roy S, Ezati P, Rhim J-W. Gelatin/carrageenan-based functional films with carbon dots from enoki mushroom for active food packaging applications. ACS Applied Polymer Materials. 2021;3(12):6437-45.

49. Fu B, Liu Q, Liu M, Chen X, Lin H, Zheng Z, et al. Carbon dots enhanced gelatin/chitosan bio-nanocomposite packaging film for perishable foods. Chinese Chemical Letters. 2022;33(10):4577-82.

811 50. Dashipour A, Razavilar V, Hosseini H, Shojaee-Aliabadi S, German JB, Ghanati K, et al.
812 Antioxidant and antimicrobial carboxymethyl cellulose films containing Zataria multiflora
813 essential oil. International journal of biological macromolecules. 2015;72:606-13.
814 51. De Sanctis F, Silvestrini MG, Luneia R, Botondi R, Bellincontro A, Mencarelli F.
815 Postharvest dehydration of wine white grapes to increase genistein, daidzein and the main
816 carotenoids. Food chemistry. 2012;135(3):1619-25.
817 52. Moradi M, Tajik H, Rohani SMR, Mahmoudian A. Antioxidant and antimicrobial effects
818 of zein edible film impregnated with Zataria multiflora Boiss. essential oil and monolaurin. LWT-
819 Food Science and Technology. 2016;72:37-43.
820 53. Dong X, Liang W, Meziani MJ, Sun Y-P, Yang L. Carbon dots as potent antimicrobial
821 agents. Theranostics. 2020;10(2):671.
822 54. Kim YH, Kim GH, Yoon KS, Shankar S, Rhim J-W. Comparative antibacterial and
823 antifungal activities of sulfur nanoparticles capped with chitosan. Microbial Pathogenesis.
824 2020;144:104178.
825 55. Ezati P, Rhim J-W, Molaei R, Priyadarshi R, Roy S, Min S, et al. Preparation and
826 characterization of B, S, and N-doped glucose carbon dots: Antibacterial, antifungal, and
827 antioxidant activity. Sustainable Materials and Technologies. 2022;32:e00397.
828 56. Sharififar F, Moshafi M, Mansouri S, Khodashenas M, Khoshnoodi M. In vitro evaluation
829 of antibacterial and antioxidant activities of the essential oil and methanol extract of endemic
830 Zataria multiflora Boiss. Food control. 2007;18(7):800-5.
831 57. Rubilar JF, Cruz RM, Zuñiga RN, Khmelinskii I, Vieira MC. Mathematical modeling of
832 gallic acid release from chitosan films with grape seed extract and carvacrol. International journal
833 of biological macromolecules. 2017;104:197-203.

58. Ezati P, Rhim J-W, Molaei R, Priyadarshi R, Han S. Cellulose nanofiber-based coating film integrated with nitrogen-functionalized carbon dots for active packaging applications of fresh fruit. Postharvest Biology and Technology. 2022;186:111845.

59. Lucero-Acuña A, Gutiérrez-Valenzuela CA, Esquivel R, Guzmán-Zamudio R. Mathematical modeling and parametrical analysis of the temperature dependency of control drug release from biodegradable nanoparticles. RSC advances. 2019;9(16):8728-39.

60. Ranjbaryan S, Pourfathi B, Almasi H. Reinforcing and release controlling effect of cellulose nanofiber in sodium caseinate films activated by nanoemulsified cinnamon essential oil. Food Packaging and Shelf Life. 2019;21:100341.

61. Chen K, Zhang M, Bhandari B, Deng D. 3D printed cinnamon essential oil/banana peel carbon dots loaded corn starch/gelatin bilayer film with enhanced functionality for food packaging application. Food Chemistry. 2024;448:139176.

Tables

Table1. Physical, barrier and mechanical properties of Persian Gum-based film and date seeds CQDs at different concentrations (0.5, 1 and 1.5%)*.

Film	Thickness (µm)	WS (%)	WVP (g.m/m2.Pa.s × 10^{-10})	Tensile strength (MPa)	Elongation at break (%)	Elastic modulus (MPa)
Control	62.12 ± 3.46^{ab}	42.44 ± 0.35^{b}	10.78 ± 0.76^{c}	0.357 ± 0.02^{c}	17.826 ± 4.81^{b}	6.730 ± 2.12^{c}
CD1	55.35 ± 2.3^{b}	51.06 ± 0.14^{ab}	29.82 ± 1.18^{ab}	0.536 ± 0.16^{bc}	20.841 ± 6.27^{b}	7.241 ± 3.04^{c}
CD2	54.4 ± 3.08^{b}	53.74 ± 0.47^{a}	37.45 ± 2.09^{a}	1.361 ± 0.23^{a}	34.717 ± 2.36^{a}	26.670 ± 7.86^{ab}
CD3	54.16 ± 1.89^{b}	54.13 ± 0.83^{a}	39.66 ± 1.27^{a}	1.005 ± 0.15^{ab}	28.496 ± 5.18^{ab}	21.479 ± 3.77^{b}
E	68.52 ± 2.7^{a}	29.64 ± 0.13^{c}	8.40 ± 1.22^{c}	0.871 ± 0.19^{b}	23.462 ± 3.37^{b}	18.442 ± 5.26^{b}
CD/E	64.11 ± 4.2^{a}	40.37 ± 0.56^{b}	25.09 ± 3.34^{b}	1.827 ± 0.38^{a}	41.079 ± 2.24^{a}	30.453 ± 2.48^{a}

*The values are presented as mean ± standard deviation. Any two means in the same column followed by the same letter are not significantly ($p > 0.05$) different by Duncan's multiple range tests.

Different letters in the same column indicate significant differences between the control and nanocomposite treatment ($P < 0.05$).

Table 2. Surface color and light transmittance of the Persian Gum-based films and date seeds CQDs at different concentrations (0.5, 1 and 1.5%)*.

Films	L^*	a^*	b^*	ΔE	T_{280} (%)	T_{660} (%)
PG	77.51 ± 0.01^{a}	-0.36 ± 0.02^{a}	18.95 ± 0.07^{d}	2.08 ± 0.20^{d}	10.34 ± 0.64^{a}	62.33 ± 0.94^{a}
PG/CQD$^{0.5}$	66.62 ± 2.3^{b}	-0.38 ± 0.02^{a}	27.56 ± 0.38^{c}	7.57 ± 0.19^{c}	6.75 ± 0.48^{b}	58.31 ± 0.88^{b}
PG/CQD$^{1.0}$	60.73 ± 1.22^{c}	-0.83 ± 0.01^{b}	33.92 ± 0.47^{b}	12.69 ± 0.09^{a}	1.39 ± 0.06^{c}	56.16 ± 0.73^{b}
PG/CQD$^{1.5}$	52.19 ± 0.98^{d}	-1.18 ± 0.08^{c}	37.34 ± 0.36^{a}	17.9 ± 0.59^{b}	0.003 ± 0.01^{d}	49.25 ± 0.46^{c}

*The values are presented as mean ± standard deviation. Any two means in the same column followed by the same letter are not significantly ($p > 0.05$) different by Duncan's multiple range tests.

Table 3. Antimicrobial and antioxidant properties of Persian gum-based nanocomposites at different CQDs concentrations (0.5, 1 and 1.5%) and ZMEO (1.5%)*.

Treatments	Inhibition zone (mm)**				Antioxidant activity (%)
	S. aureus	*E. coli*	*L. monocytogenes*	*S. typhimurium*	
Control	-	-	-	-	4.85 ± 0.18^{d}
CD1	6.5 ± 0.1^{d}	-	-	-	28.06 ± 1.19^{c}
CD2	21.5 ± 1.0^{bc}	15.0 ± 0.5^{ab}	18.5 ± 1.0^{b}	19.5 ± 0.5^{b}	39.25 ± 2.43^{b}
CD3	23.5 ± 2.0^{a}	18.5 ± 1.5^{a}	23.5 ± 1.0^{a}	20.0 ± 2.0^{ab}	40.33 ± 3.2^{b}
E	22.5 ± 1.0^{bc}	16.5 ± 0.5^{ab}	21.5 ± 0.5^{ab}	20.5 ± 0.5^{ab}	54.12 ± 2.96^{ab}
CD/E	25 ± 2.0^{b}	17.5 ± 1.0^{a}	23.0 ± 1.5^{a}	22.0 ± 1.0^{a}	63.48 ± 4.55^{a}

*The values are presented as mean ± standard deviation. [a-d] Means in the same column shown with different letters are significantly different ($P < 0.05$).

Table 4. Parameters of models for ZMEO release from nanocomposite films containing different concentrations of CQDs at 4, 25 and 37 ˚C.

Temperature		**Model**											
		Zero order		**First order**		**Higuchi**		**Korsmeyer-Peppas**			**Peleg**		
	Treatment	K	R^2	K	R^2	K	R^2	K	n	R^2	K_1	K_2	R^2
4 ˚C	**0.5%CQD**	0.009	0.882	0.00	0.911	0.599	0.962	0.508	0.318	0.977	7.05	0.024	0.984
	1%CQD	0.008	0.869	0.00	0.897	0.509	0.953	0.490	0.306	0.968	7.183	0.027	0.986
	1.5%CQD	0.008	0.618	0.00	0.829	0.452	0.921	0.464	0.304	0.958	7.293	0.031	0.996
25 ˚C	**0.5%CQD**	0.017	0.734	0.00	0.841	1.153	0.878	1.176	0.236	0.954	1.533	0.010	0.999
	1%CQD	0.012	0.680	0.00	0.748	0.811	0.830	1.183	0.203	0.920	1.54	0.013	0.999
	1.5%CQD	0.009	0.723	0.00	0.769	0.635	0.868	1.152	0.187	0.951	1.775	0.016	0.999
37 ˚C	**0.5%CQD**	0.011	0.421	-0.004	0.455	0.824	0.602	1.008	0.227	0.722	1.103	0.015	0.987
	1%CQD	0.007	0.368	-0.003	0.476	0.561	0.544	0.986	0.268	0.752	1.184	0.019	0.994
	1.5%CQD	0.007	0.406	-0.002	0.433	0.525	0.587	0.935	0.236	0.747	1.342	0.021	0.994

Figure captions

Fig 1. Schematic illustration for the preparation of CDs.

Fig. 2. (A) TEM image and (B) particle size distribution picture of CQDs.

Fig. 3. FTIR spectra of PG-based film and its nanocomposites at different amounts of CQDs obtained from DS (0.5-1.5% wt).

Fig 4. UV–visible light (a) transmittance and (b) absorbance of persian gum films added with CQDs from date seed at different levels.

Fig 5. SEM images of (a) surface and (b) cross-section of persian gum -based films.

Fig. 6. The effects of time, temperature and CQD concentration on the release pattern of ZMEO from PG films at three temperatures of 4, 25 and 37 ˚C.

Figures

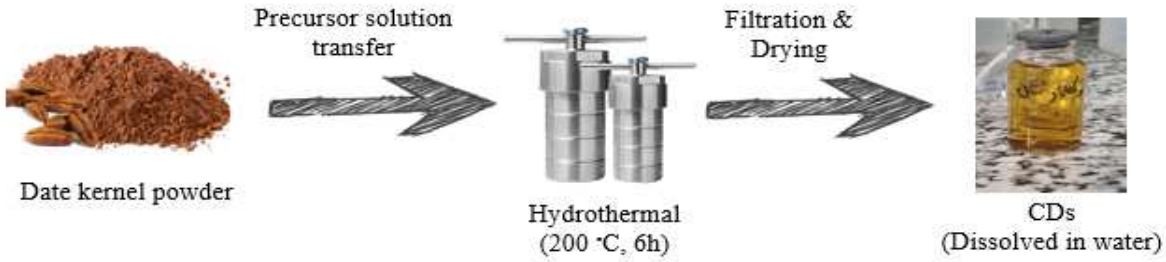


Fig. 1

A) B)

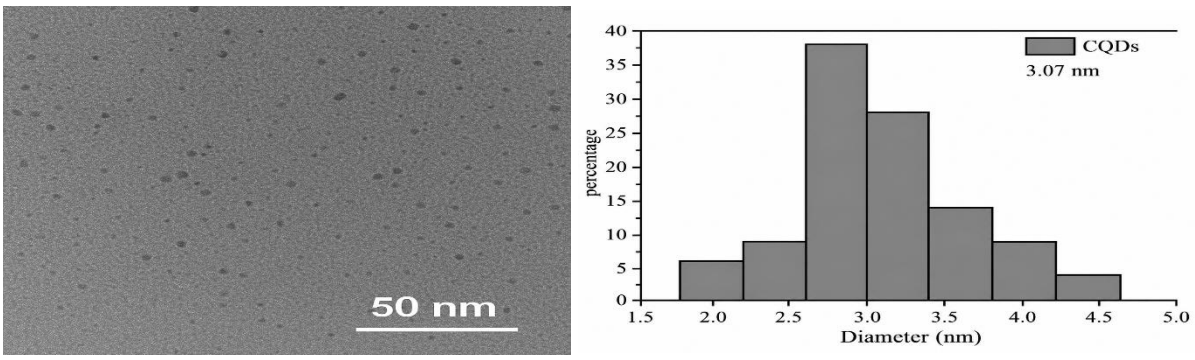

50 nm
CQDs
3.07 nm
percentage
Diameter (nm)
0
5
10
15
20
25
30
35
40
1.5
2.0
2.5
3.0
3.5
4.0
4.5
5.0

Fig. 2

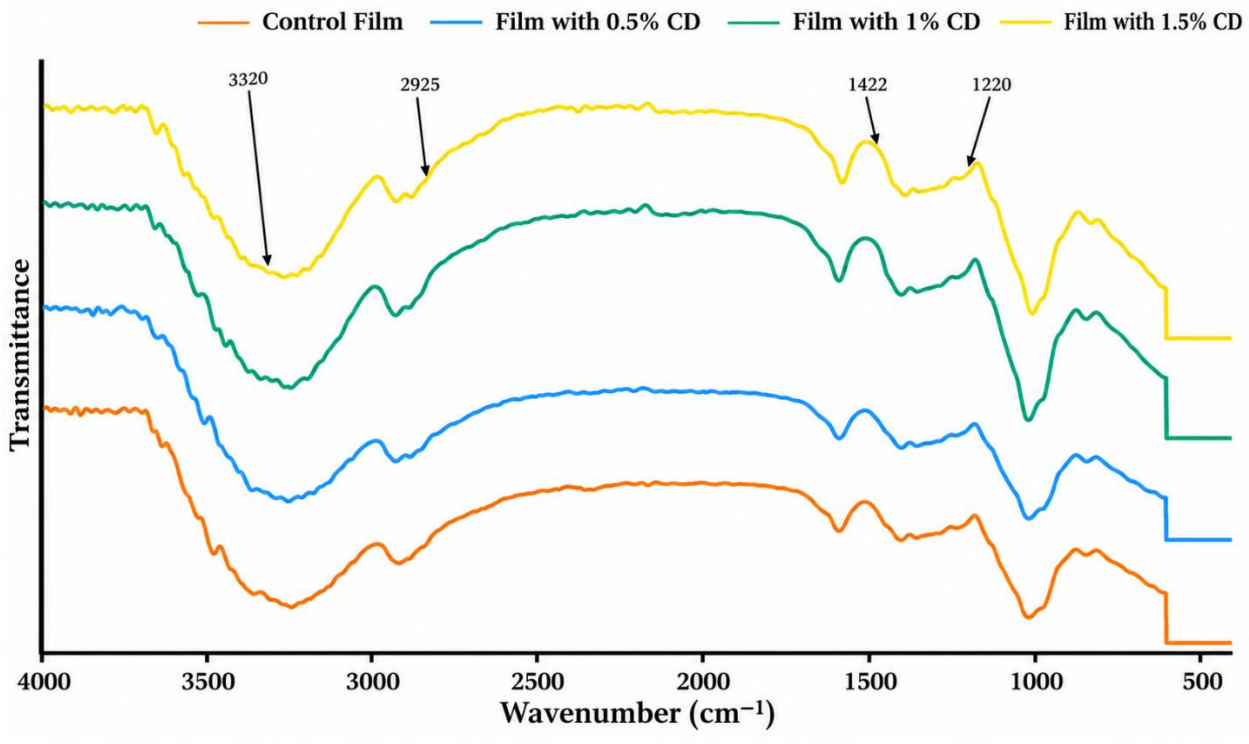
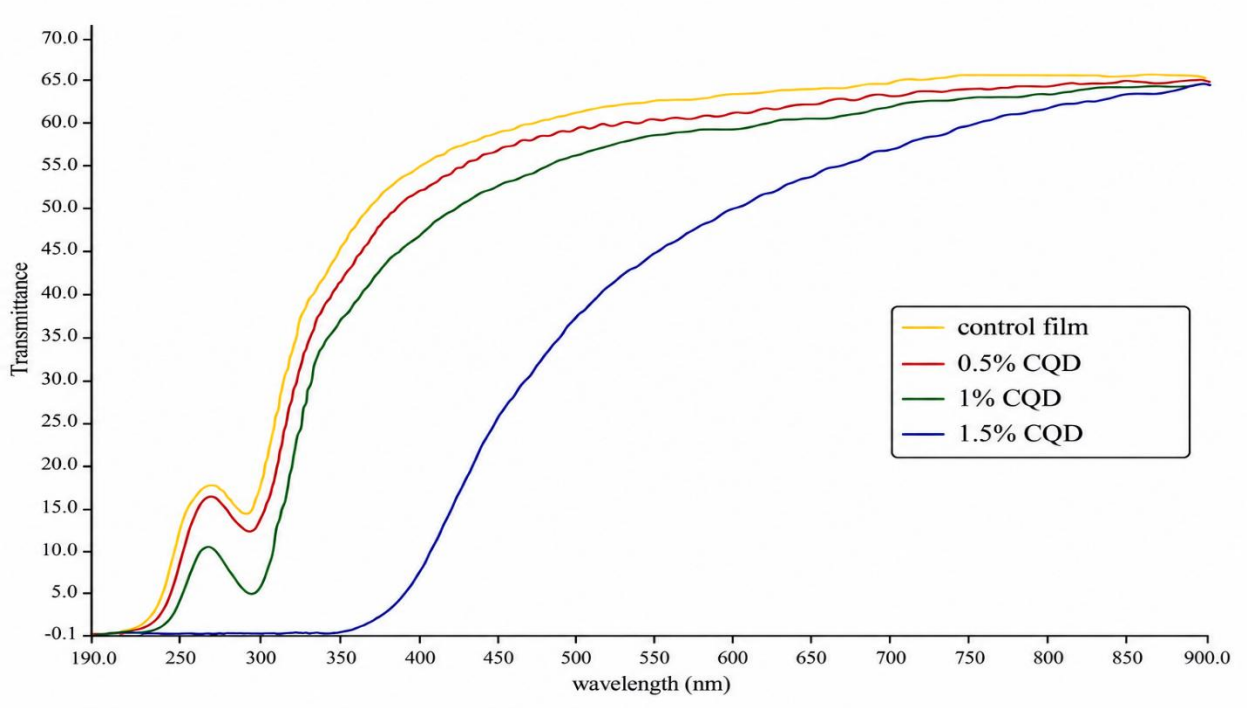

Control Film
Film with 0.5% CD
Film with 1% CD
Film with 1.5% CD
3320
2925
1422
1220
Transmittance
4000
3500
3000
2500
2000
1500
1000
500
Wavenumber (cm⁻¹)

Fig. 3

(a


Transmittance
70.0
65.0
60.0
55.0
50.0
45.0
40.0
35.0
30.0
25.0
20.0
15.0
10.0
5.0
-0.1
190.0
250
300
350
400
450
500
550
600
650
700
750
800
850
900.0
wavelength (nm)
control film
0.5% CQD
1% CQD
1.5% CQD

(b)

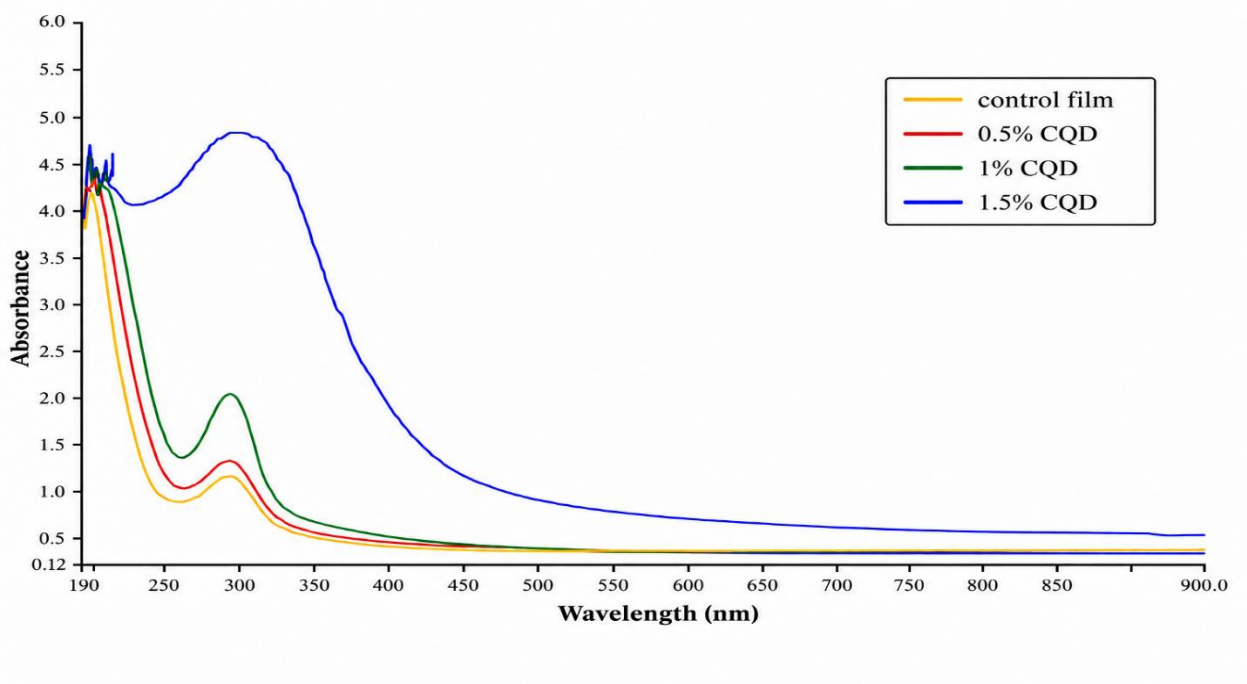
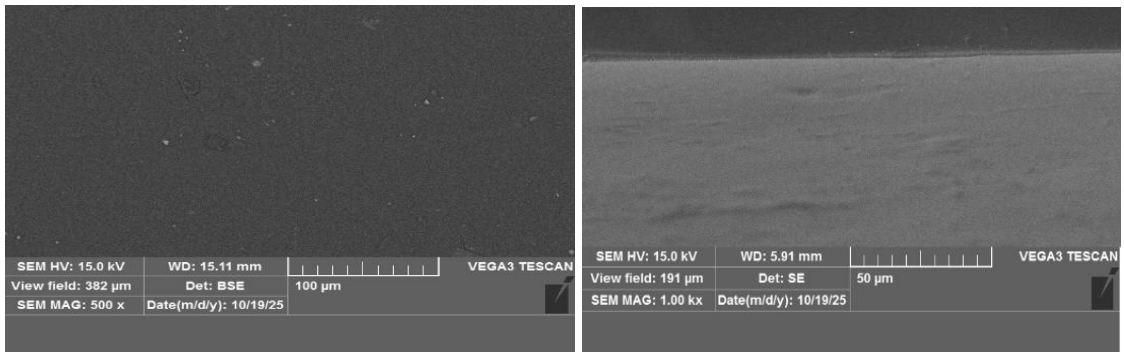


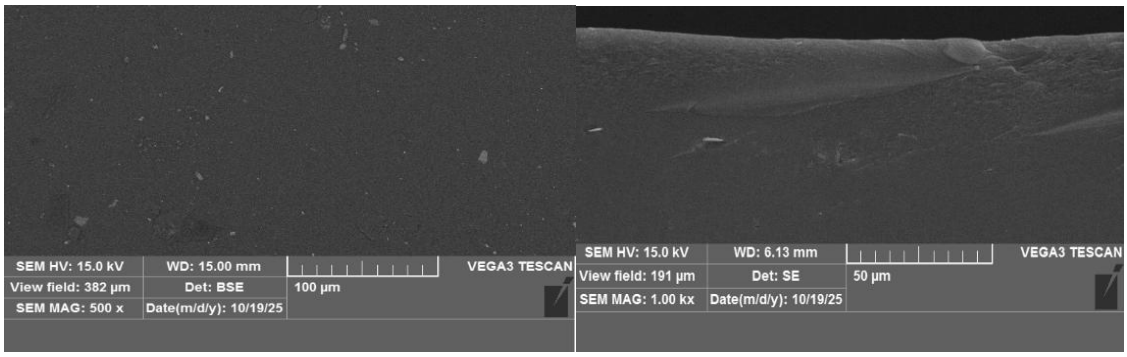
Fig. 4

a) **b)**

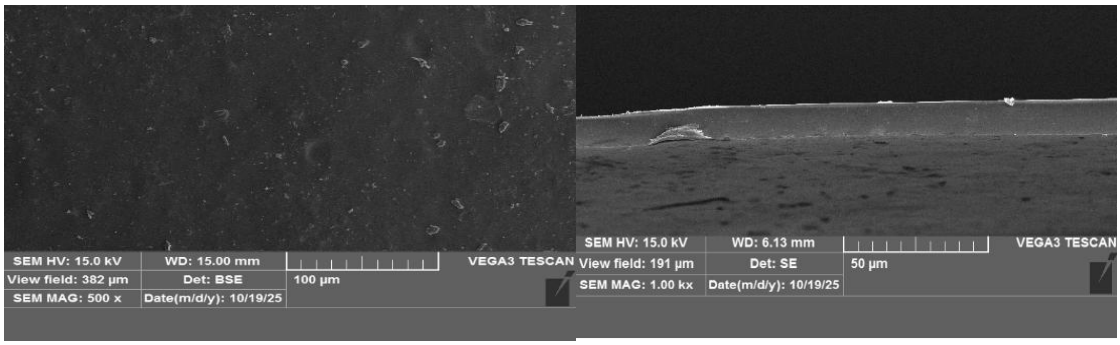
Control



CD



CD/E



1049

1050 **Fig. 5**

1051

1052

1053

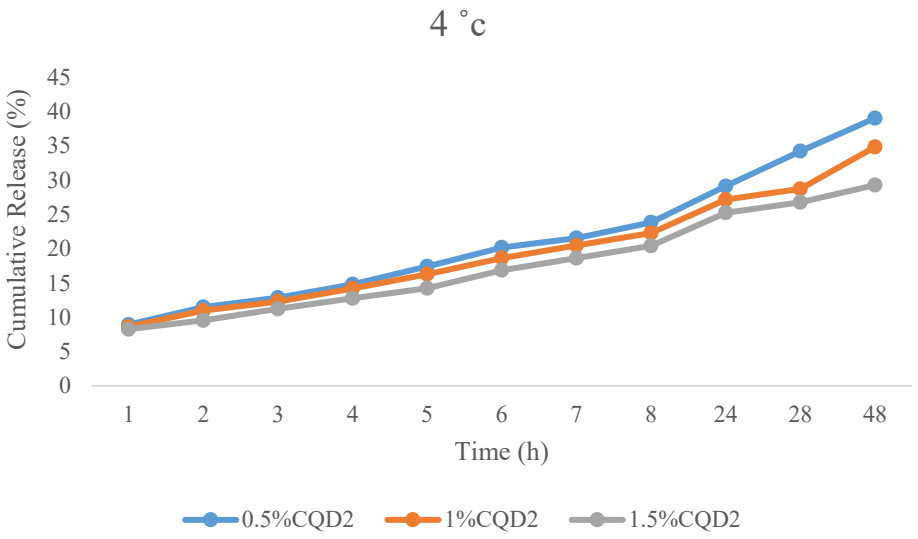
1054

1055

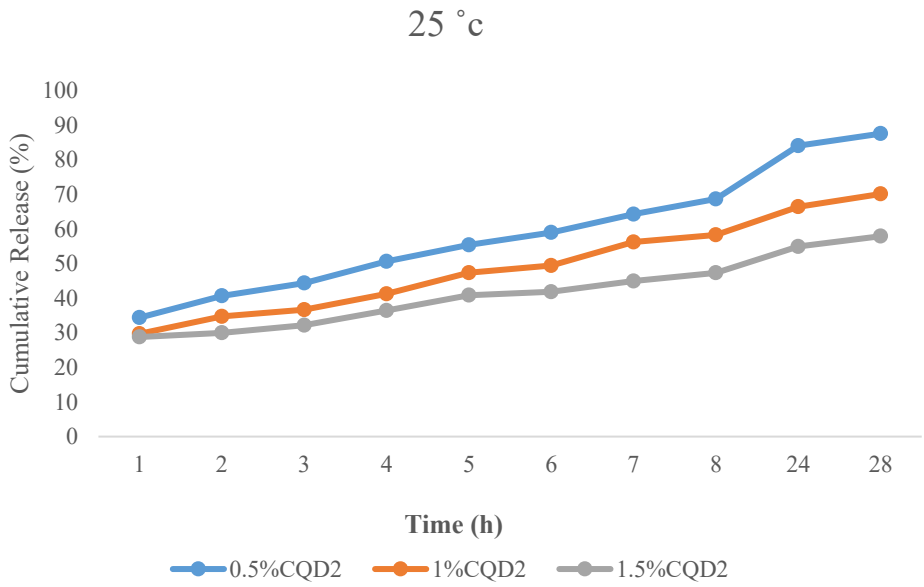
1056

1057

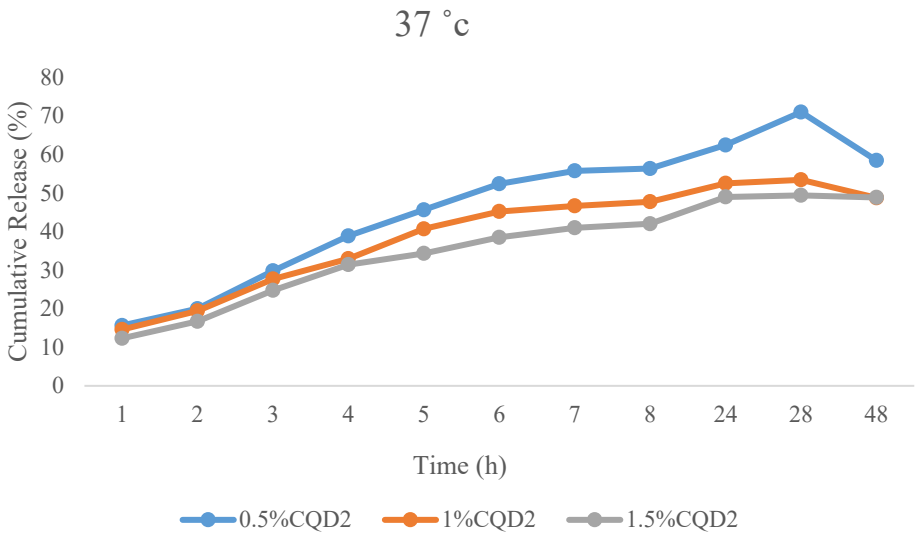
1058


4 ˚c
Cumulative Release (%)
45
40
35
30
25
20
15
10
5
0
1
2
3
4
5
6
7
8
24
28
48
Time (h)
0.5%CQD2
1%CQD2
1.5%CQD2

1059


25 ˚c
Cumulative Release (%)
100
90
80
70
60
50
40
30
20
10
0
1
2
3
4
5
6
7
8
24
28
Time (h)
0.5%CQD2
1%CQD2
1.5%CQD2

1060



1061
1062 **Fig. 6**

1063